# Double-layer coating containing boron nitride powder for efficient daytime radiative cooling

**Satoshi Ishii,[1,2,*] Etsuko Shimada[1], Ryugo Hosokawa[1,2], Minoru Morioka[3], Motoharu Fukazawa[3], Takashi Kawasaki[3]**

[1] Research Center for Materials Nanoarchitectonics (MANA), National Institute for Materials Science (NIMS), 1-1 Namiki, Tsukuba, Ibaraki 305-0044, Japan.

[2] Faculty of Pure and Applied Physics, University of Tsukuba, Tsukuba, Ibaraki 305-8577, Japan.

[3] New Business Development, Denka Co., Ltd., Chuo-ku, Tokyo 103-8338, Japan

*E-mail address: sishii@nims.go.jp

Keywords: radiative cooling, thermal radiation, thermal conductivity, boron nitride

## Abstract

Daytime radiative cooling outdoors is a passive cooling method that emits thermal radiation toward the sky while reflecting sunlight. Many different daytime radiative coolers have been developed, and some have been commercialized. Coatings offer advantages in ease of application and versatility across different surfaces. Typical daytime radiative cooling coatings are mixtures of powders or particles in polymer hosts. As these paintings reflect sunlight diffusively, the coating thicknesses are sub-millimeters or thicker. Thick coatings result in high thermal resistance, which is undesirable for cooling the objects below the coating. To address this problem, boron nitride (BN) powder has been used as a material with high thermal conductivity to reduce thermal resistance. However, the high refractive index of BN in the mid-infrared regions prevents the mid-infrared emissivity of BN-containing coatings from achieving values above 0.9 if the concentration is high. In the current work, we demonstrate a high average emissivity reaching 0.93 and solar reflectance of 0.99 by adding a layer containing silica powder where the silica layer is instrumental in enhancing the emissivity without deteriorating the solar reflectance. The double-layer coatings exhibit subambient outdoor temperatures in Japan. Introducing a silica layer for thermal emission on top of a BN-containing base layer presents a straightforward method to enhance the daytime radiative cooling performance of the BN-containing layer.

## Introduction

Global warming and social trends toward decarbonization have been significant forces behind renewable energy. In addition to renewable energy sources, passive methods have attracted significant attention because they do not consume electrical energy. Regarding cooling and heat dissipation, radiative cooling to the sky by thermal radiation is a passive outdoor method. In particular, daytime radiative coolers have been the main target of research because they can cool in daytime in which cooling is required the most because of solar heating.[1-6] The two key requirements for daytime radiative cooling are high solar reflectance and high mid-infrared (MIR) emissivity. Since the early works of the past century,[7, 8] many different types of daytime radiative coolers have been studied, including multilayers,[9-13] natural materials,[14-16] porous materials,[17-21] and sheets.[22, 23] Among daytime radiative coolers, powders dispersed in polymers[24, 25] are simple to prepare and can be coated on any surface, making them more robust and attractive.

While coatings of powder-dispersed polymers are simple and easy to fabricate, large thicknesses are necessary to achieve near 100% solar reflectance because high reflectance is due to multiple scattering inside the coating. The thicknesses of the coatings ranged from a few hundred microns to more than 1 mm.[25-30] This starkly contrasts to a silver thin film that can reflect more than 90% of sunlight with 100-nm thickness. Because commonly used powders such as silica ($SiO_2$) and titania and polymers such as acrylic have relatively low thermal conductivities, thick coatings lead to significant thermal resistances. A coating with high thermal resistance hinders heat transfer from the inner side to the outer surface facing the sky.

Recent studies have attempted to lower the thermal resistance of coatings by choosing a powder material with high thermal conductivity and a large bandgap exceeding 3.5 eV. Boron nitride (BN) is a material that meets these requirements, and BN powders have already been used in daytime radiative coolers.[28, 31-38] High solar reflectance and high thermal conductivities compared to other daytime radiative coolers have been demonstrated, however, their average emissivity values were lower than 0.9 if the concentration is high owing to the high refractive index of BN [39, 40]

In the current study, a $SiO_2$ layer was added to the BN layer to improve its emissivity while maintaining its high solar reflectance. The top $SiO_2$ layer was kept thin to avoid deterioration of the high solar reflectance of the underlying BN layer. Recent studies have applied double layers in daytime radiative coolers.[24] In most cases, the purpose of forming double layers is to enhance the UV reflectance of the underlying titania layers that absorb in the UV range.[30, 41, 42] Layer thicknesses and polymers were varied to find an optimized layer combination. When PMMA was used as the polymer for BN powder, the solar reflectance and average emissivity reached 0.99 and 0.92, respectively. When CYTOP was chosen as the polymer for the BN powder, solar reflectance and average emissivity were 0.99 and 0.93, respectively, with thinner thickness than with PMMA host. Outdoor measurements confirmed

the subambient cooling of the samples. Paintable daytime radiative cooler has an advantage in covering large areas. Having high thermal conductivity is advantageous when cooling electronic devices.[38]

## Results and discussion

Although the focus of the current work is to use high thermal conductivity powder in daytime radiative cooler, it is imperative to have high solar reflectance and high average emissivity. For quantitative comparison, solar reflectance is defined as,

$$R_{\mathrm{solar}} = \frac{\int_{0.3\mu\mathrm{m}}^{2.5\mu\mathrm{m}} I_{\mathrm{AM1.5}}(\lambda) R(\lambda) d\lambda}{\int_{0.3\mu\mathrm{m}}^{2.5\mu\mathrm{m}} I_{\mathrm{AM1.5}}(\lambda) d\lambda}, \quad (1)$$

where $\lambda$, $I_{\mathrm{AM1.5}}$, and $R$ are wavelength, air mass 1.5 spectrum of sunlight, and defused reflectance, respectively. In addition, the average emissivity within the atmospheric window is defined as,

$$\varepsilon_{\mathrm{ave}} = \frac{\int_{8\mu\mathrm{m}}^{13\mu\mathrm{m}} I_{\mathrm{BB}}(T,\lambda) \varepsilon(\lambda) d\lambda}{\int_{8\mu\mathrm{m}}^{13\mu\mathrm{m}} I_{\mathrm{BB}}(T,\lambda) d\lambda}, \quad (2)$$

where $I_{\mathrm{BB}}$ and $\varepsilon$ are blackbody thermal emission at 300 K and emissivity of the sample. Using solar reflectance and average emissivity, a figure of merit (*FoM*) has been introduced.[26] The *FoM* for a daytime radiative cooler was calculated using solar reflectance and average emissivity as follows;

$$FoM = \varepsilon_{\mathrm{ave}} - r(1 - R_{\mathrm{solar}}), \quad (3)$$

where *r* is the ratio of solar irradiation to blackbody emission, which was set to 10 as Japan is not a dry area.[26] The comparison based on the *FoM* does not depend on weather or measurement location, thus enabling fair comparison.

At the beginning of the study, wide bandgap ceramic powders, including $SiO_2$, alumina ($Al_2O_3$), and aluminum nitride (AlN), were investigated in addition to BN to compare their radiative cooling performances. More than one powder with different average diameters was prepared for each powder material. Each powder was mixed with polymethyl methacrylate (PMMA) at the highest concentration which did not exhibit cracks when forming the film (see Table S1). A high concentration was chosen because a higher concentration generally results in a higher reflectance. Each film thickness was adjusted to 0.5 mm by polishing. A summary of nine different powders is shown in Table 1. The comparison shows that the BN powders have higher solar reflectances than the others; however, their average emissivities are inferior to those of other materials. Among the BN powders, the one whose average diameter is 24.8 μm has the highest solar reflectance. Note that the BN powder with 3.0 μm average diameter was too fine to fabricate a crack-free film in PMMA.

Table 1. Solar reflectance and average emissivity of various ceramic powders dispersed in PMMA. Each coating thickness is 0.5 mm and coated on an Al plate. With BN(3.0 μm), a crack-free film was not formed, thus no data for BN(3.0 μm).

| Powder | Solar reflectance | Average emissivity |
|---|---|---|
| $SiO_2$(6.6 μm) | 0.94 | 0.923 |
| $SiO_2$(45.2 μm) | 0.82 | 0.91 |
| $Al_2O_3$(5.1 μm) | 0.88 | 0.93 |
| $Al_2O_3$(96.3 μm) | 0.76 | 0.89 |
| AlN(3.7 μm) | 0.80 | 0.92 |
| AlN(94.1 μm) | 0.73 | 0.91 |
| BN(3.0 μm) | NA | NA |
| BN 6.1 μm) | 0.97 | 0.76 |
| BN(24.8 μm) | 0.98 | 0.81 |

In the following, BN powder having 24.8 μm diameter (hereafter, BN(24.8 μm)) was investigated further. Figure 1(a) shows the thickness dependence of BN(24.8 μm) in PMMA (hereafter, BN(24.8 μm)/PMMA). A slight increase in solar reflectance was observed as the film thickness increased. The average emissivity did not increase above 0.9, even though the thickness was 2.5 mm. These results suggest that achieving solar reflectance above 0.98 and average emissivity above 0.90 with only a BN layer is impossible.

One way to overcome the limitation of BN powder is to form double layers. The bottom layer contains BN powder, and the top layer must be thin enough so that the partially transmitted sunlight can take advantage of the high solar reflectance of the bottom BN-containing layer. At the same time, the top layer must have a higher emissivity than the BN-containing layer. To search for an appropriate powder for use as the top layer, $SiO_2$, $Al_2O_3$ and AlN powders were tested as the top layers. The concentrations were identical to those reported in Table 1, and all thicknesses were fixed at 0.3 mm. The solar reflectance, average emissivity, and *FoM* values are listed in Table S2. Among the six samples, the double layer having $SiO_2$(6.6 μm) layer on the top has the highest *FoM*, and this *FoM* is higher than the *FoM* for single BN layer. The thickness dependence of $SiO_2$(6.6 μm)/PMMA layer on the top on a BN(24.8 μm)/PMMA was tested and plotted in Figure 1(b). The highest solar reflectance is obtained when the top $SiO_2$(6.6 μm)/PMMA thickness is 0.3 mm. Although the average emissivity increases with increasing $SiO_2$(6.6 μm)/PMMA thickness, a 0.3-mm thick layer gives the highest *FoM* as solar reflectance impacts the *FoM* more than the average emissivity.

From the above investigations, BN(24.8 μm)/PMMA(2.0 mm)+$SiO_2$(6.6 μm)/PMMA(0.3 mm) turned out to be the best double layers using PMMA as the BN powder host. The schematic and photo of BN(24.8 μm)/PMMA(2.0 mm)+$SiO_2$(6.6 μm)/PMMA(0.3 mm) are shown in Figures 1(c) and 1(d), respectively. The photo shows the coating's whitish appearance.

Figure 2 shows the defused reflectance in the UV-visible-NIR and emissivity in the MIR for the BN(24.8 μm)/PMMA(2.0 mm) and BN(24.8 μm)/PMMA(2.0 mm)+$SiO_2$(6.6 μm)/PMMA(0.3 mm). By comparing the reflectance emissivity of the two samples, the spectra show an emissivity increase while maintaining the high reflectance by adding the silica layer ($SiO_2$(6.6 μm)/PMMA(0.3 mm)).

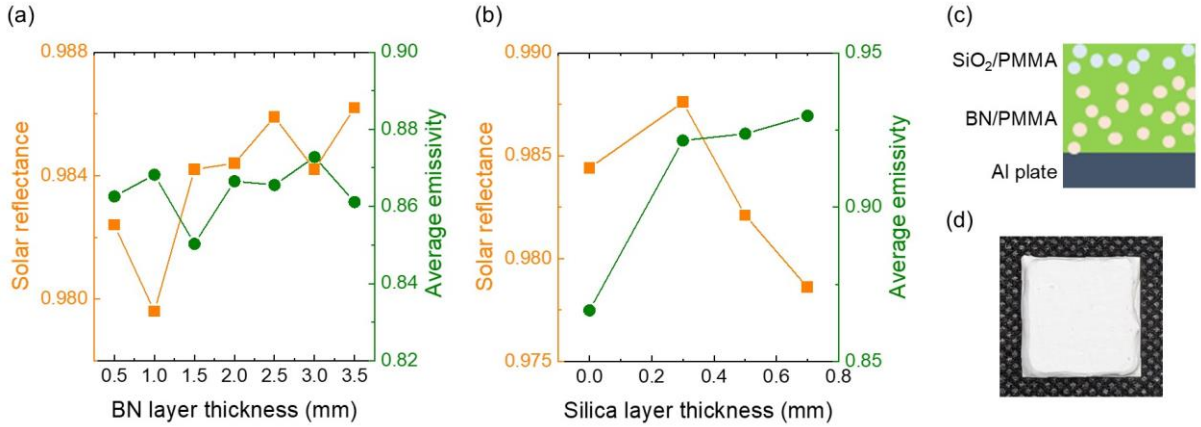


Figure 1. Solar reflectance and average emissivity for (a) BN(24.8 μm)/PMMA layer having various thicknesses, and (b) BN(24.8 μm)/PMMA(2 mm)+$SiO_2$(6.6 μm)/PMMA having various $SiO_2$(6.6 μm)/PMMA thicknesses. (c) Schematic and (d) photo of BN(24.8 μm)/PMMA(2 mm)+$SiO_2$(6.6 μm)/PMMA(0.3 mm).

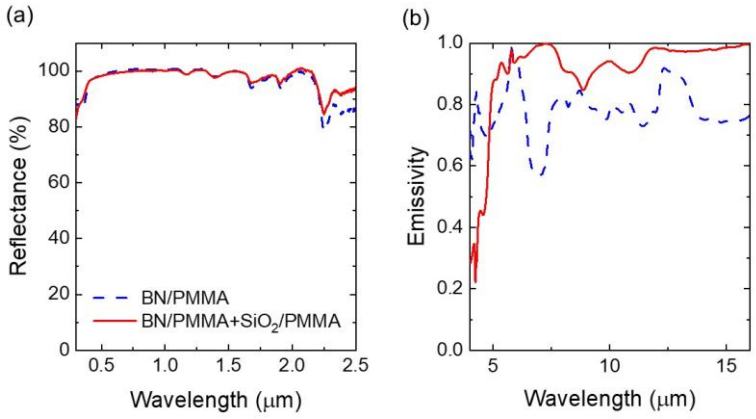


Figure 2. (a) Defused reflectance in the UV-visible-NIR range, and (b) emissivity in the MIR of BN(24.8 μm)/PMMA(2.0 mm) and BN(24.8 μm)/PMMA(2.0 mm)+$SiO_2$(6.6 μm)/PMMA(0.3 mm) which are abbreviated as BN/PMMA and BN/PMMA+$SiO_2$/PMMA, respectively, in the legend.

Another strategy to improve the low emissivity of the BN layer is to mix BN and $SiO_2$ powder. With this regard, BN(24.8 μm) and $SiO_2$(6.6 μm) powders at various ratios ranging from 5:0 to 0:5 were weighted and subsequently mixed into PMMA to form layers. The total weight of each powder sample was fixed. The solar reflectance and average emissivity of the

six layers having 0.5 mm thicknesses are shown in Figure S1. As the $SiO_2$ ratio increased, the solar reflectance decreased as an overall trend. These results show that a mixture of BN and $SiO_2$ powder cannot overcome the low average emissivity of a single BN layer without decreasing the solar reflectance.

For the first set of experiments presented earlier, PMMA was the host matrix. Another polymer, CYTOP, was explored in a subsequent set of experiments. CYTOP is a fluoropolymer that is transparent from UV to near-infrared (NIR) and has a refractive index of 1.34 (at 589 nm), which is lower than that of commonly available polymers, including PMMA (refractive index = 1.49 at 589 nm).[43] A lower refractive index gives a higher refractive index contrast between the host and powder, resulting in higher scattering. Hence, replacing PMMA with CYTOP is expected to reduce the thickness of the layer.

Figure 3(a) shows the thickness dependence of BN(24.8 μm) mixed in CYTOP (labeled as BN(24.8 μm)/CYTOP). The x-axis range differs from the one in Figure 1(a) due to the difference in PMMA and CYTOP refractive indexes. As long as the thickness is equal or greater than 0.5 mm, the solar reflectance is larger than 0.99. Higher solar reflectance with a thinner thickness than the BN(24.8 μm)/PMMA is attributed to the lower refractive index of CYTOP. The average emissivity of BN(24.8 μm)/CYTOP is lower than 0.8, thus a single layer of BN(24.8 μm)/CYTOP is not suitable, which is similar to BN(24.8 μm)/PMMA.

Similar to the BN(24.8 μm)/PMMA configuration, a SiO2(6.6 μm)/PMMA layer was added to the BN(24.8 μm)/CYTOP(0.8 mm) structure. Note that CYTOP was tested as a host for $SiO_2$(6.6 μm), however, obtaining a crack-free coating with CYTOP was impossible in our study. Their resultant solar reflectance and average emissivity are shown in Figure 3(b). Incorporating the $SiO_2$ (6.6 μm)/PMMA layer resulted in the average emissivity exceeding 0.9, which is higher than that of the single layer of BN(24.8 μm)/CYTOP. The solar reflectance is the highest when the $SiO_2$(6.6 μm)/PMMA thickness is 0.1 mm, and it gradually decreases as the thickness increases. The increase in average emissivity and decrease in solar reflectance are attributed to the features of the $SiO_2$(6.6 μm)/PMMA layer.

The above investigations indicate that BN(24.8 μm)/CYTOP(0.8 mm)+$SiO_2$(6.6 μm)/PMMA(0.1 mm) is the best double layer when CYTOP is used as a host for BN powder. The schematic and photo of BN(24.8 μm)/CYTOP(0.8 mm)+$SiO_2$(6.6 μm)/PMMA(0.1 mm) are shown in Figures 3(c) and 1(d), respectively. A whitish appearance is seen in the photo. Figure S2 shows the defused reflectance in the UV-visible-NIR and emissivity in the MIR for the BN(24.8 μm)/CYTOP(0.8 mm) and BN(24.8 μm)/CYTOP(0.8 mm)+$SiO_2$(6.6 μm)/PMMA(0.1 mm). Similar to the samples with PMMA host for BN(24.8 μm), adding a silica layer increased the emissivity while maintaining the high reflectance.

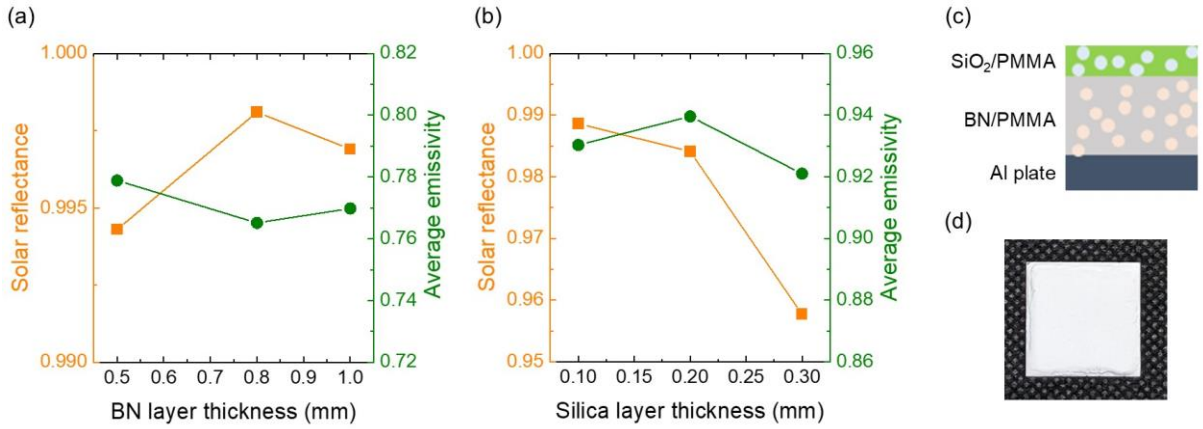


Figure 3. Solar reflectance and average emissivity for (a) BN(24.8 μm)/CYTOP having various thicknesses, and (b) BN(24.8 μm)/CYTOP(0.8 mm)+$SiO_2$ (6.6 μm)/PMMA having valuable $SiO_2$ (6.6 μm)/PMMA thicknesses. (c) Schematic and (d) photo of BN(24.8 μm)/CYTOP(0.8 mm)+$SiO_2$ (6.6 μm)/PMMA(0.1 mm).

In addition to the optical characterization, the films' thermal properties were measured and listed in Table 2. The incorporation of BN powder improved the thermal conductivity more than four times compared to pure PMMA and CYTOP. Qualitatively, this can be understood as the powders having higher thermal conductivity than the polymers; incorporating the powder into polymers increased the composite film's thermal conductivity. As the thermal conductivity of BN is higher than that of silica, higher thermal conductivity is obtained for BN(24.8 μm)/PMMA than $SiO_2$(6.6 μm)/PMMA. In reality, BN has an extremely high thermal conductivity in the in-plane direction (220-450 W/m/K) and much lower in the through-plane direction (2.5-5.5 W/m/K).[44] From the top-view SEM images in Figure 4, more than half of the BN powders were oriented in-plane (i.e. perpendicular to the thickness direction). As the thermal diffusivity was measured along the thickness direction, the through-plane thermal conductivity of BN contributed more to the measured value. Aligning the powder parallel to the thickness direction may lead to higher thermal conductivity.

Table 2. Thermal conductivities of polymers mixed with powders and polymers.

| | Thermal conductivity (W/m/K) |
|---|---|
| BN(24.8 μm)/PMMA | 0.86 |
| BN(24.8 μm)/CYTOP | 0.67 |
| $SiO_2$(6.6 μm)/PMMA | 0.44 |
| PMMA | 0.20 |
| CYTOP | 0.12 |

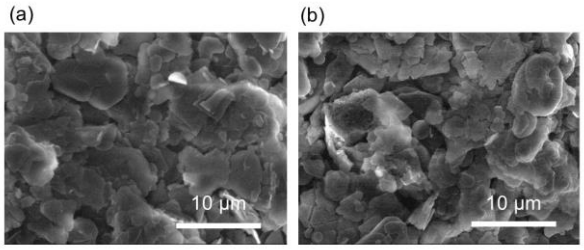


Figure 4. SEM images of (a) BN(24.8 μm)/PMMA and (b) BN(24.8 μm)/CYTOP.

From the above investigations, BN(24.8 μm)/PMMA(2.0 mm)+$SiO_2$(6.6 μm)/PMMA(0.3 mm) and BN(24.8 μm)/CYTOP(0.8 mm)+$SiO_2$ (6.6 μm)/PMMA(0.1 mm) turned out to be the best double layers using PMMA and CYTOP as the BN powder host, respectively. Hereafter, BN(24.8 μm)/PMMA(2.0 mm)+$SiO_2$(6.6 μm)/PMMA(0.3 mm) and BN(24.8 μm)/CYTOP(0.8 mm)+$SiO_2$(6.6 μm)\/PMMA(0.1 mm) are shortened as, BN/PMMA+$SiO_2$/PMMA and BN/CYTOP+$SiO_2$/PMMA, respectively. Outdoor daytime radiative cooling performances were tested in Tsukuba, Japan, in October 2022 (Figure S3). The results are presented with the ambient temperature and solar irradiance in Figures 5(b)-(c) and Figure 5(c)-(d) for BN/PMMA+$SiO_2$/PMMA and BN/CYTOP+$SiO_2$/PMMA, respectively. The vertical axes of Figures 5(a) and 5(c) show the temperature difference between the sample and ambient, where the sample temperatures were measured at the back side of the substrates. Negative values indicate that the samples were cooler than the ambient temperature, even without windshields. Figures S4(a) and S4(b) show the temperature differences of the single layer samples (BN/PMMA and BN/CYTOP), Al plates, and blackbody samples measured at the same time with BN/PMMA+$SiO_2$/PMMA and BN/CYTOP+$SiO_2$/PMMA, respectively. The Al plates and blackbody samples were chosen as representative samples for solar reflectors and solar absorbers, respectively. Not only were the double-layer samples cooler than the Al plates and blackbody samples, but they were also cooler than the single-layer samples. This indicates that the $SiO_2$ effectively worked for radiative cooling by increasing the emissivity of the samples.

For the double-layer samples, the magnitude of the temperature differences decreased in the afternoon, as seen in Figures 5(a) and 5(c). For Figure 5(a), the reason is most likely due to the appearance of the clouds, which is indicated by a decrease in solar irradiance in Figure 5(b). For Figure 5(c), the reason is probably caused by the stronger wind speed in the afternoon than in the morning (see Figure S5). Although the temperature differences were small in the afternoon, the outdoor measurements confirmed that the samples had daytime cooling abilities. Additionally, numerical heat transfer simulations[13] were performed to model the temperature differences between the sample and ambient, and the results are also shown in Figures 5(a) and 5(c) for both samples. Some discrepancies between the measured and simulated temperature exist, however, overall time dependences agree well, verifying that the cooling was caused by

heat transfer to the sky.

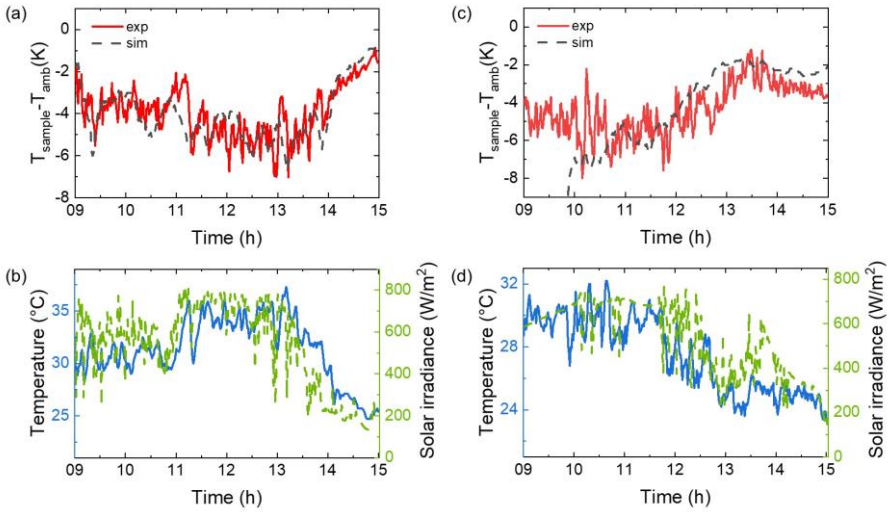


Figure 5. (a) Measured and numerically simulated temperature difference between the sample ($T_{sample}$) and ambient ($T_{amb}$) for BN/PMMA+$SiO_2$/PMMA placed outdoors. (b) Ambient temperature (solid line) and solar irradiance (dash line) during the outdoor measurement on October 11th, 2022, in Tsukuba, Japan. (c) Measured and numerically simulated temperature difference between the sample and ambient for BN/CYTOP+$SiO_2$/PMMA placed outdoors. (d) Ambient temperature (solid line) and solar irradiance (dash line) during the outdoor measurement on October 21st, 2022, in Tsukuba, Japan. The sizes of the samples on the photos are both 2 cm square.

In the end, the *FoM* values of BN/PMMA+$SiO_2$/PMMA and BN/CYTOP+$SiO_2$/PMMA are listed in Table S3. Four other BN-containing polymers and $BaSO_4$-containing polymer which is reported to have the highest solar reflectance among paintable daytime radiative coolers are added in Table S3 for comparison. Our BN-containing double layers had higher *FoMs* than others because of higher average emissivity. As the fabrication of our films is merely mixing and coating, it is scalable to cover a large area. Additionally, our work proved that if a film has high solar reflectance but has low average emissivity, its emissivity can be improved by adding a thin film with low sunlight absorption and high emissivity. This strategy can be applied to other types of radiative cooling films which have high solar reflectance but have low average emissivity.

## Conclusion

Daytime radiative coolers containing BN powder in the host polymers were developed. To maintain the high solar reflectance of the BN-containing layer and enhance its emissivity, a thin polymer layer containing $SiO_2$ powder was added. The double layer achieved both high solar reflectance and high average emissivity. When PMMA was used as the host polymers for the BN powder, the solar reflectance and average emissivity were 0.99 and 0.92, respectively.

When CYTOP was used as the host polymer for the BN powder, the solar reflectance and average emissivity were 0.99 and 0.93, respectively. The outdoor measurements confirmed that BN/PMMA+ $SiO_2$/PMMA and BN/CYTOP+$SiO_2$/PMMA were cooled by thermal radiation during the day, and the double-layer coolers were more efficient than the coolers without silica layers. A comparison based on the *FoM* indicated that the double layers were superior to those of previously reported powder-incorporated polymers. As the developed double layers can be formed similar to paints, they can be formed over a large area for practical applications.

**Sample fabrication**

BN(3.0 μm), BN(6.1 μm), $SiO_2$(6.6 μm), $SiO_2$(45.2 μm), $Al_2O_3$(5.1 μm), $Al_2O_3$(96.3 μm), powders were obtained from Denka Co. Ltd. BN(24.8 μm) powder, PMMA and anisole were purchased from FUJIFILM Wako Pure Chemical Corporation. AlN(3.7 μm) and AlN(94.1 μm) powders were obtained from Furukawa Electric Co., Ltd.. CYTOP(CTL-107MK) was purchased from AGC Inc.. To dissolve PMMA, 1 g of PMMA was mixed with 10 ml anisole in an oil bath which was kept at 50 °C for more than an hour. CYTOP was used as its original concentration without dilution. Each powder and polymer solution were weighed with the ratio shown in Table S1 and mixed by a magnetic starler for a few minutes. The mixture was coated on a 0.2-mm thick aluminum (Al) plate to form a layer. The coating was repeated when aiming for a large thickness. The coated layer was dried on a hotplate kept at 120 °C for a few minutes. To adjust the thickness, the surface was scraped with a metal file.

**Optical characterization**

The defused reflectance spectra in the UV-visible-NIR range were measured using a UV-VIS spectrometer (V-770, JASCO) with an integrating sphere. The reflectance of each sample was normalized using a Spectralon. Defused reflectance spectra in the MIR range were obtained using by an FITR (Nicolet iS50R FT-IR, Thermo Fisher Scientific K.K.) equipped with a gold-coated integrating sphere (Upward IntegratIR, PIKE Technologies, Inc.). The reflectance of each sample was normalized to that of a gold-coated rough surface provided by PIKE Technologies, Inc.. The emissivity was calculated by subtracting defused reflectance from unity.

**Outdoor measurement**

The outdoor measurement settings were similar to the one reported earlier.[13] The thermocouple was attached to each sample's bottom side (i.e., Al plate) with a 40-μm-thick double-sided tape. The four corners of the sample bottom were gently suspended using a circular hole in a plastic sample mount covered with Al foil to reflect sunlight. The samples were firmly placed facing the coated side up by fixing the thermocouple with the plastic sample mount. The plastic sample mount was placed on an approximately 3-cm thick polystyrene foam covered with Al foil and placed on the roof of the five-story building at the National Institute of Materials Science

(36°04'07.8"N, 140°07'58.7"E). Windshields, often used by others, were not used to ensure that the top surfaces of the samples were exposed to atmospheric conditions, which resulted in the fluctuation of sample temperature. In addition to the double-layer samples (BN/PMMA+$SiO_2$/PMMA and BN/CYTOP+$SiO_2$/PMMA), single BN layer samples (BN/PMMA and BN/CYTOP), bare Al plates, and blackbody-paint coated Al plates were also placed outside, and their temperatures were recorded.

During the measurements, the temperature and humidity were recorded using a logger whose sensor head was covered with Al foil and placed next to the sample (within 10 cm). The solar irradiance was measured by a pyranometer placed within 1.0 m from the samples. Downward radiation (i.e., atmospheric radiation) data and ten-minute average wind speed data were recorded at the Aerological Observatory in Tsukuba, Japan. The distance between the National Institute of Materials Science and the Aerological Observatory was approximately 2 km; therefore, the weather conditions at the two locations were assumed to be similar.

**Author contributions**

S.I. conceived the idea of the experiments. S.E., R.H. and S.I. carried out sample fabrication and characterization. S.I. did the numerical simulations. All the authors were involved in the discussion and manuscript writing.

**Corresponding Author**

E-mail: sishii@nims.go.jp

**ORCID**

Satoshi Ishii: 0000-0003-0731-8428

Ryugo Hosokawa: 0009-0001-7579-4752

**Competing interests**

The authors declare no competing interests.

**Supporting Information**

Volume fractions, solar reflectance, and average emissivity of the films; reflectance and emissivity spectra and SEM images of the films; photos of the outdoor measurement setting; temperature difference of the samples measured outdoors.

**Acknowledgment**

S.I. acknowledges the financial support from JST PRESTO (JPMJPR19I2), JST FOREST (JPMJFR2139) and Kakenhi from JSPS (22H01917), Japan.

## Data Availability

The raw data required to reproduce the above findings are available upon request.

## References


1. Zeyghami, M.; Goswami, D. Y.; Stefanakos, E., A review of clear sky radiative cooling developments and applications in renewable power systems and passive building cooling. *Sol. Energy Mater Sol. Cells* **2018,** *178*, 115-128.
2. Zhao, B.; Hu, M.; Ao, X.; Chen, N.; Pei, G., Radiative cooling: A review of fundamentals, materials, applications, and prospects. *Appl. Energy* **2019,** *236*, 489-513.
3. Zhao, D.; Aili, A.; Zhai, Y.; Xu, S.; Tan, G.; Yin, X.; Yang, R., Radiative sky cooling: Fundamental principles, materials, and applications. *Appl. Phys. Rev.* **2019,** *6* (2).
4. Yin, X.; Yang, R.; Tan, G.; Fan, S., Terrestrial radiative cooling: Using the cold universe as a renewable and sustainable energy source. *Science* **2020,** *370* (6518), 786-791.
5. Chen, M.; Pang, D.; Chen, X.; Yan, H.; Yang, Y., Passive daytime radiative cooling: Fundamentals, material designs, and applications. *EcoMat* **2022,** *4* (1), e12153.
6. Fan, S.; Li, W., Photonics and thermodynamics concepts in radiative cooling. *Nat. Photo.* **2022,** *16* (3), 182-190.
7. Catalanotti, S.; Cuomo, V.; Piro, G.; Ruggi, D.; Silvestrini, V.; Troise, G., The radiative cooling of selective surfaces. *Sol. Energy* **1975,** *17* (2), 83-89.
8. Granqvist, C. G.; Hjortsberg, A., Radiative cooling to low temperatures: General considerations and application to selectively emitting SiO films. *J. Appl. Phys.* **1981,** *52* (6), 4205-4220.
9. Raman, A. P.; Anoma, M. A.; Zhu, L.; Rephaeli, E.; Fan, S., Passive radiative cooling below ambient air temperature under direct sunlight. *Nature* **2014,** *515* (7528), 540-544.
10. Kou, J.-l.; Jurado, Z.; Chen, Z.; Fan, S.; Minnich, A. J., Daytime Radiative Cooling Using Near-Black Infrared Emitters. *ACS Photonics* **2017,** *4* (3), 626-630.
11. Suichi, T.; Ishikawa, A.; Hayashi, Y.; Tsuruta, K., Performance limit of daytime radiative cooling in warm humid environment. *AIP Adv.* **2018,** *8* (5).
12. Chae, D.; Kim, M.; Jung, P.-H.; Son, S.; Seo, J.; Liu, Y.; Lee, B. J.; Lee, H., Spectrally Selective Inorganic-Based Multilayer Emitter for Daytime Radiative Cooling. *ACS Appl. Mater. Interfaces* **2020,** *12* (7), 8073-8081.
13. Ishii, S.; Hernández-Pinilla, D.; Tanjaya, N. K.; Nagao, T., Highly reflective multilayer solar reflectors for daytime radiative cooling. *Sol. Energy Mater Sol. Cells* **2023,** *259*, 112463.
14. Li, T.; Zhai, Y.; He, S.; Gan, W.; Wei, Z.; Heidarinejad, M.; Dalgo, D.; Mi, R.; Zhao, X.; Song, J.; Dai, J.; Chen, C.; Aili, A.; Vellore, A.; Martini, A.; Yang, R.; Srebric, J.; Yin, X.; Hu, L., A radiative cooling structural material. *Science* **2019,** *364* (6442), 760-763.

15. Chen, Y.; Dang, B.; Fu, J.; Wang, C.; Li, C.; Sun, Q.; Li, H., Cellulose-Based Hybrid Structural Material for Radiative Cooling. *Nano Lett.* **2021,** *21* (1), 397-404.
16. Tian, Y.; Shao, H.; Liu, X.; Chen, F.; Li, Y.; Tang, C.; Zheng, Y., Superhydrophobic and Recyclable Cellulose-Fiber-Based Composites for High-Efficiency Passive Radiative Cooling. *ACS Appl. Mater. Interfaces* **2021,** *13* (19), 22521-22530.
17. Mandal, J.; Fu, Y.; Overvig, A. C.; Jia, M.; Sun, K.; Shi, N. N.; Zhou, H.; Xiao, X.; Yu, N.; Yang, Y., Hierarchically porous polymer coatings for highly efficient passive daytime radiative cooling. *Science* **2018,** *362* (6412), 315-319.
18. Leroy, A.; Bhatia, B.; Kelsall, C. C.; Castillejo-Cuberos, A.; Di Capua H., M.; Zhao, L.; Zhang, L.; Guzman, A. M.; Wang, E. N., High-performance subambient radiative cooling enabled by optically selective and thermally insulating polyethylene aerogel. *Sci. Adv.* **2019,** *5* (10), eaat9480.
19. Wang, X.; Liu, X.; Li, Z.; Zhang, H.; Yang, Z.; Zhou, H.; Fan, T., Scalable Flexible Hybrid Membranes with Photonic Structures for Daytime Radiative Cooling. *Adv. Funct. Mater.* **2020,** *30* (5), 1907562.
20. Lee, D.; Go, M.; Son, S.; Kim, M.; Badloe, T.; Lee, H.; Kim, J. K.; Rho, J., Sub-ambient daytime radiative cooling by silica-coated porous anodic aluminum oxide. *Nano Energy* **2021,** *79*, 105426.
21. Wang, Y.; Wang, T.; Liang, J.; Wu, J.; Yang, M.; Pan, Y.; Hou, C.; Liu, C.; Shen, C.; Tao, G.; Liu, X., Controllable-morphology polymer blend photonic metafoam for radiative cooling. *Materials Horizons* **2023,** *10* (11), 5060-5070.
22. Zhai, Y.; Ma, Y.; David, S. N.; Zhao, D.; Lou, R.; Tan, G.; Yang, R.; Yin, X., Scalable-manufactured randomized glass-polymer hybrid metamaterial for daytime radiative cooling. *Science* **2017,** *355* (6329), 1062-1066.
23. Yang, R.; Xie, F.; Li, Y.; Wang, X.; Pan, Y.; Liu, C.; Shen, C.; Liu, X., Advancing thermal comfort: an innovative $SiO_2$ microsphere-decorated shish-kebab film composite for enhanced personal cooling. *Advanced Nanocomposites* **2024,** *1* (1), 86-93.
24. Bao, H.; Yan, C.; Wang, B.; Fang, X.; Zhao, C. Y.; Ruan, X., Double-layer nanoparticle-based coatings for efficient terrestrial radiative cooling. *Sol. Energy Mater Sol. Cells* **2017,** *168*, 78-84.
25. Li, X.; Peoples, J.; Yao, P.; Ruan, X., Ultrawhite BaSO4 Paints and Films for Remarkable Daytime Subambient Radiative Cooling. *ACS Appl. Mater. Interfaces* **2021,** *13* (18), 21733-21739.
26. Li, X.; Peoples, J.; Huang, Z.; Zhao, Z.; Qiu, J.; Ruan, X., Full Daytime Sub-ambient Radiative Cooling in Commercial-like Paints with High Figure of Merit. *Cell Rep. Phys. Sci.*. **2020,** *1* (10), 100221.
27. Zhang, Y.; Tan, X.; Qi, G.; Yang, X.; Hu, D.; Fyffe, P.; Chen, X., Effective radiative cooling with ZrO2/PDMS reflective coating. *Sol. Energy Mater Sol. Cells* **2021,** *229*,

111129.
28. Li, P.; Wang, A.; Fan, J.; Kang, Q.; Jiang, P.; Bao, H.; Huang, X., Thermo-Optically Designed Scalable Photonic Films with High Thermal Conductivity for Subambient and Above-Ambient Radiative Cooling. *Adv. Funct. Mater.* **2022,** *32* (5), 2109542.
29. Mabchour, G.; Benlattar, M.; Saadouni, K.; Mazroui, M., Optically selective PDMS/AIN coatings as a passive daytime radiative cooling design. *Mater. Today: Proc.* **2022,** *66*, 390-395.
30. Dong, Y.; Zou, Y.; Li, X.; Wang, F.; Cheng, Z.; Meng, W.; Chen, L.; Xiang, Y.; Wang, T.; Yan, Y., Introducing masking layer for daytime radiative cooling coating to realize high optical performance, thin thickness, and excellent durability in long-term outdoor application. *Appl. Energy* **2023,** *344*, 121273.
31. Yang, Z.; Zhou, Z.; Sun, H.; Chen, T.; Zhang, J., Construction of a ternary channel efficient passive cooling composites with solar-reflective, thermoemissive, and thermoconductive properties. *Compos. Sci. Technol.* **2021,** *207*, 108743.
32. Felicelli, A.; Katsamba, I.; Barrios, F.; Zhang, Y.; Guo, Z.; Peoples, J.; Chiu, G.; Ruan, X., Thin layer lightweight and ultrawhite hexagonal boron nitride nanoporous paints for daytime radiative cooling. *Cell Rep. Phys. Sci.*. **2022,** *3* (10), 101058.
33. Zhao, J.; Meng, Q.; Li, Y.; Yang, Z.; Li, J., Structural Porous Ceramic for Efficient Daytime Subambient Radiative Cooling. *ACS Appl. Mater. Interfaces* **2023,** *15* (40), 47286-47293.
34. Zhang, W.; Wang, Y.; Sun, H.; Liu, C.; Shen, C.; Liu, X., Thermal conductive high-density polyethylene/boron nitride composites with high solar reflectivity for radiative cooling. *Adv. Compos. Hybrid Mater.* **2023,** *6* (5), 163.
35. Chang, S.-W.; Chen, Y.-J.; Wan, D.; Chen, H.-L., Near-room-temperature waste heat recovery through radiative cooling for both daytime and nighttime power generation. *J. Mater. Chem. A* **2023,** *11* (28), 15183-15195.
36. Wang, S.; Wu, Y.; Pu, M.; Xu, M.; Zhang, R.; Yu, T.; Li, X.; Ma, X.; Su, Y.; Tai, H.; Guo, Y.; Luo, X., A Versatile Strategy for Concurrent Passive Daytime Radiative Cooling and Sustainable Energy Harvesting. *Small* **2024,** *20* (6), 2305706.
37. Liu, S.; Zhang, F.; Chen, X.; Yan, H.; Chen, W.; Chen, M., Thin paints for durable and scalable radiative cooling. *J. Energy Chem.* **2024,** *90*, 176-182.
38. Zhao, X.; Tang, G. H., 0D/2D Co-Doping Network Enhancing Thermal Conductivity of Radiative Cooling Film for Electronic Device Thermal Management. *ACS Appl. Mater. Interfaces* **2024,** *16* (29), 37853-37864.
39. Geick, R.; Perry, C. H.; Rupprecht, G., Normal Modes in Hexagonal Boron Nitride. *Phys. Rev.* **1966,** *146* (2), 543-547.
40. Cai, Y.; Zhang, L.; Zeng, Q.; Cheng, L.; Xu, Y., Infrared reflectance spectrum of BN calculated from first principles. *Solid State Commun.* **2007,** *141* (5), 262-266.

41. Lin, K.; Du, Y.; Chen, S.; Chao, L.; Him Lee, H.; Chung Ho, T.; Zhu, Y.; Zeng, Y.; Pan, A.; Yan Tso, C., Nanoparticle-polymer hybrid dual-layer coating with broadband solar reflection for high-performance daytime passive radiative cooling. *Energ. Buildings* **2022,** *276*, 112507.
42. Zhao, B.; Xu, C.; Jin, C.; Lu, K.; Chen, K.; Li, X.; Li, L.; Pei, G., Superhydrophobic bilayer coating for passive daytime radiative cooling. *Nanophotonics* **2023**.
43. Inc., A. CYTOP® - Downloads: CYTOP® Low refractive index. https://www.agc-chemicals.com/file.jsp?id=file/Cytop_tech13_EN.pdf.
44. Jiang, P.; Qian, X.; Yang, R.; Lindsay, L., Anisotropic thermal transport in bulk hexagonal boron nitride. *Phys. Rev. Mater.* **2018,** *2* (6), 064005.

**TOC**